Freeform LED lens for rectangularly prescribed illumination

2009 J. Opt. A: Pure Appl. Opt. 11 105501

(http://iopscience.iop.org/1464-4258/11/10/105501)

J. Opt. A: Pure Appl. Opt. **11** (2009) 105501 (10pp) doi:10.1088/1464-4258/11/10/105501

Freeform LED lens for rectangularly prescribed illumination

Kai Wang[1,2], Sheng Liu[1,2,3], Fei Chen[1,2], Zong Qin[1,2], Zongyuan Liu[1,3] and Xiaobing Luo[1,4]

[1] Division of MOEMS, Wuhan National Laboratory for Optoelectronics, Wuhan 430074, People's Republic of China
[2] School of Optoelectronics Science and Engineering, Huazhong University of Science and Technology, Wuhan 430074, People's Republic of China
[3] Institute for Microsystems, School of Mechanical Science and Engineering, Huazhong University of Science and Technology, Wuhan 430074, People's Republic of China
[4] School of Energy and Power Engineering, Huazhong University of Science and Technology, Wuhan 430074, People's Republic of China

E-mail: victor_liu63@126.com (Sheng Liu)

Received 11 February 2009, accepted for publication 2 June 2009
Published 6 August 2009
Online at stacks.iop.org/JOptA/11/105501

Abstract
Freeform lenses are playing a more and more important role in LED secondary optics design. In this study, based on the new light energy mapping relationship, edge ray principle, Snell's law and error control of surface construction, a modified discontinuous freeform lens design method was presented for rectangularly prescribed illumination, with the advantages of a flexible energy mapping relationship, accurate light irradiation control and easier to manufacture. A polymethyl methacrylate (PMMA) discontinuous freeform lens was designed as an example for LED tunnel illumination according to this method. The numerical simulation results demonstrated that the light pattern of the lens was in good agreement with the expected illumination performance when using a point source. Tolerance analyses were also conducted. An extended light source had little effect on the light output efficiency (LOE) of the lens but significantly decreased the effective illumination area. Installation errors had more effect on the uniformity and shape of the light pattern than the LOE of the lens. The tolerances of vertical, horizontal and rotational deviation of this lens were 0.4 mm, 0.4 mm and 2°, respectively.

Keywords: freeform lens, light emitting diode (LED), prescribed illumination, tolerance analysis

(Some figures in this article are in colour only in the electronic version)

1. Introduction

Theoretically, the light-emitting diode (LED) has many advantages, such as low-power consumption, high reliability, long lifetime, variable color and environmental protection [1]. Since LEDs' lumen efficiency has increased rapidly in recent years, LEDs have begun to play an important role in many applications, such as backlighting for LCD display, street and tunnel lighting, and interior illumination [2, 3]. Rectangular light patterns are popular in these LED applications. However, the light patterns of most LEDs are circularly symmetric with non-uniform illuminance distribution, which makes it hard to meet the requirements of illumination. Therefore, appropriate secondary optics are essential for high quality LED illumination.

A freeform lens is a kind of newly emerging nonimaging optics and has become a trend in LED secondary optics design due to its advantages in unique design freedom, small size and accurate light irradiation control [4–12]. To deal with freeform lens design, many different methods have been proposed, such as the simultaneous multiple surfaces (SMS) method [4, 5], tailored freeform surface method [6], light energy mapping method [7, 8] and discontinuous freeform lens method [9–12], to name a few. At present, only the SMS

method could deal with an extended light source effectively. The SMS method provides an optical system with two freeform surfaces that deflects the rays of the input bundles into the rays of the corresponding output bundles and vice versa. In this paper, we will only discuss the point light source problem. A practical design method in 3D is to establish light energy mapping relationships between the light source and the target. Parkyn [8] made rectangular and warped polar grids both on the light source and the target and then matched two grids on the Gaussian sphere at the location of the luminaire-lens. Wang *et al* [9] and Ding *et al* [10, 11] obtained the mapping relationship by finding the solution of the energy conservation differential equation. Although this method provides an accurate mathematical expression between coordinates of the light source and target, it will become complicated to handle light sources with random light intensity distribution curves (LIDC), non-rectangular target grids and to find these solutions when dealing with uniform illumination problems. Moreover, the discontinuous freeform lens described in [10, 11] was constructed by 450 sub-surfaces, which are difficult to manufacture in practice.

In this paper, a modified discontinuous freeform lens design method in 3D is presented, with the advantages of a flexible energy mapping relationship, accurate light irradiation control and easier to manufacture. A discontinuous freeform lens with low profile and small volume was designed as an example for LED tunnel illumination by this method. The tunnel lamps are used here due to their significant importance for the urgent replacement for many tunnels in planning and construction in China. The effects of increasing the size of the LED chip and installation errors on the illumination performance, including uniformity and light output efficiency (LOE), were also discussed. The numerical simulation results demonstrated that the light pattern of the lens agreed quite well with the expected illumination performance and this modified method provided an effective way to deal with rectangular illumination problems, especially for small-size light sources.

2. Problem statement

During prescribed illumination design, in most cases, optical systems are designed based on the LIDC of light sources and the expected illuminance distributions on the target plane. As shown in figure 1, the freeform lens refracts the incident ray **I**, represented by spherical coordinates (γ, θ, ρ), into an output ray **O**. Then **O** will irradiate at the corresponding point Q (x, y, z) on the target plane. According to the energy mapping relationship, edge ray principle and Snell's law, the coordinates and normal vector of point P (x, y, z) on the surface of the freeform lens is able to be calculated. For the design and manufacturing convenience, the inner surface of the lens is designed as an inner concave spherical surface, which will not change the transmission directions of the incident light. We will focus on the construction of the outside surface of the lens in this study. This paper will provide an effective way to deal with rectangularly prescribed illumination problems.

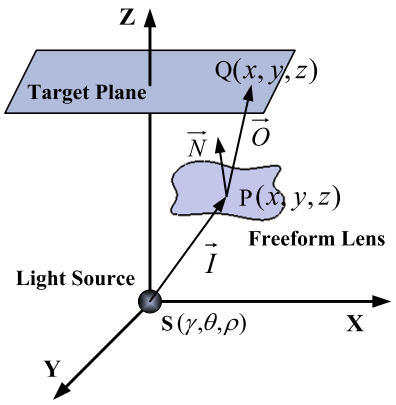

Figure 1. Schematic of the rectangularly prescribed illumination problem.

3. Design method

Since the light patterns of most LEDs are rotationally symmetric, we will only discuss this type of LED in this study. The design method includes three main parts: establishing the light energy mapping relationship between the light source and the target, constructing the lens and validating the lens design by ray tracing simulation.

3.1. Establishment of light energy mapping relationship

In this design method, light energy distribution of the light source and illumination target plane are both divided into several grids with equal luminous flux Φ_0 and area S_0, respectively. Then a mapping relationship is established between the couple of light source grid and target plane grid. Therefore, the average illuminance $E_0 = \eta\Phi_0/S_0$, where η is the light output efficiency of the freeform lens, of each target plane grid is the same and a uniform light pattern can be obtained when the grid is quite small compared with the whole target plane.

Since the light source and target plane both are of axial symmetry, only one-quarter of the whole light source and target plane are to be considered in this discussion. First of all, the light energy distribution of the light source is divided into $M \times N$ grids with equal luminous flux. As shown in figure 2, the light source's light energy distribution Ω could be regarded as being composed of a number of unit conical objects Ω_0, which represents the luminous flux within the angular range with field angle $\mathrm{d}\gamma$ in the latitudinal direction and $\mathrm{d}\theta$ in the longitudinal direction. The luminous flux of Ω_0 can be expressed as follows:

$$\phi = \int I(\theta)\,\mathrm{d}\omega = \int_{\gamma_1}^{\gamma_2} \mathrm{d}\gamma \int_{\theta_1}^{\theta_2} I(\theta)\sin\theta\,\mathrm{d}\theta \qquad (1)$$

where $I(\theta)$ is the light intensity distribution of the light source and $\mathrm{d}\omega$ is the solid angle of one unit conical object. Least-squares curve fitting in the form of a polynomial is one of the most used curve fitting methods in numerical analysis. Thus, most $I(\theta)$, expressed in the form of a light intensity

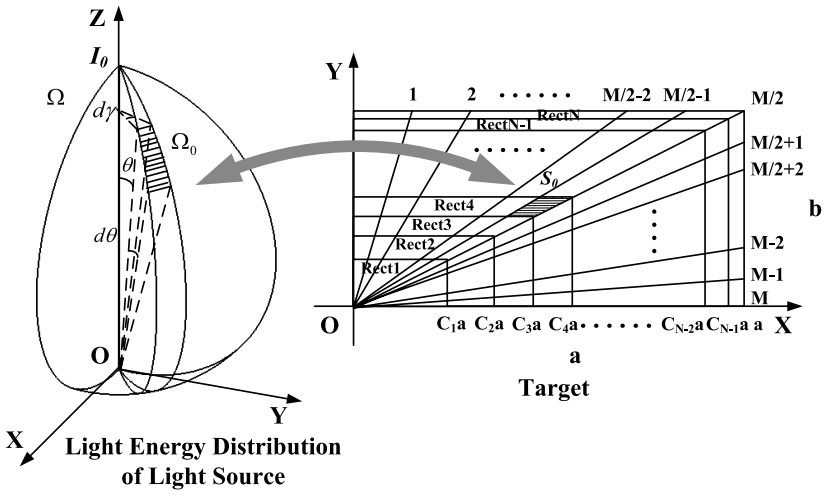

Figure 2. Schematic of light energy mapping between the light source and target.

distribution curve (LIDC), can be fitted by a polynomial of θ as follows:

$$I(\theta) = I_0 \sum_{i=0}^{m} a_i \theta^i \tag{2}$$

where I_0 is the unit light intensity, a is the polynomial coefficient and m is the order of this polynomial. The larger m is, the more accurate the curve fitting will be, but the corresponding computational work will increase too. For most LIDCs, m should not be less than 9. The total luminous flux of this one-quarter light source can be expressed as follows:

$$\phi_{\text{total}} = \int_0^{\pi/2} \mathrm{d}\gamma \int_0^{\pi/2} I(\theta) \sin\theta \, \mathrm{d}\theta = \frac{\pi}{2} \int_0^{\pi/2} I(\theta) \sin\theta \, \mathrm{d}\theta. \tag{3}$$

We divide the Ω into M fan-shaped plates along the latitudinal direction with an equal angle of $\Delta\gamma = \pi/2M$ and an equal luminous flux of Φ_{total}/M (as shown in figure 2). Then each fan-shaped plate is divided into N parts equally along the longitudinal direction. The field angle $\Delta\theta_{j+1}$, which is different for every j, of each separate conical object along the longitudinal direction can be obtained by iterative calculation as follows:

$$\frac{\pi}{2M} \int_{\theta_j}^{\theta_{j+1}} I(\theta) \sin\theta \, \mathrm{d}\theta = \frac{\phi_{\text{total}}}{MN}$$
$$(j = 0, 1, 2, \ldots, N-1, \quad \theta_0 = 0) \tag{4}$$

$$\Delta\theta_{j+1} = \theta_{j+1} - \theta_j \qquad (j = 0, 1, 2, \ldots, N-1). \tag{5}$$

Thus the light source has been divided into $M \times N$ sub-sources with equal luminous flux. The directions of rays, which define the boundary of one sub-source, have also been defined.

Secondly, to establish the mapping relationship with the light source, the one-quarter target plane is also divided into $M \times N$ grids with equal area. A warped polar grid topology [8] is appropriate to fit a rectangle. Since the target plane is perpendicular to the central axis of the light source, z is a constant Z_0 for all points on the target. As shown in figure 2, the length and width of the one-quarter rectangular target plane is a and b, respectively, and the area is $S = ab$. Firstly, the target plane is divided into N parts equally by sub-rectangles Rect1, Rect2, ..., Rect$N$, which have the same length–width ratios as the whole plane. The relationship of the area S_{Rect_k} of each sub-rectangle is

$$S_{\text{Rect}_k} = k S_{\text{Rect}_1} \qquad (k = 1, 2, \ldots, N) \tag{6}$$

where $S_{\text{Rect}_N} = S$. Therefore the rectangular target plane has been divided into N parts with the same area of S/N. The coefficient C_q of the length of $C_q a$ of each sub-rectangle can be obtained as follows:

$$C_q = \left(\frac{q}{N}\right)^{1/2} \qquad (q = 1, 2, \ldots, N). \tag{7}$$

Then the plane is divided into M parts equally along the central radiation directions by $M - 1$ radial lines. The endpoints of these lines equally divide the edges of the target plane, which ensures that the plane has been divided into M parts with equal area S/M. The edges of sub-rectangles and radial lines construct the warped polar grids. Therefore the plane has been divided into $M \times N$ grids S_0 with equal area S/MN.

According to the edge ray principle [13], rays from the edge of the source should strike the edge of the target. This principle is true in 2D, and in 3D the skew invariant will lead to loss, but which could be partly recovered by increasing the number of grids. Therefore if we desire to map the light energy in Ω_0 into the target grid S_0, we should ensure that four rays, which construct Ω_0 as the boundary, irradiate at the four corresponding end points of the target grid S_0 after being refracted by the freeform lens. Since the light source and target plane are both divided into $M \times N$ grids, each ray from the light source could only have one corresponding irradiated point on the target plane. Thus the light energy mapping relationship between the light source and target plane has been established. When dealing with non-rectangular illumination problems, it only needs to change the size and shape of the grids on the target plane, which makes it more easy and flexible to re-establish the light energy mapping relationships comparing with the methods mentioned in [9–11].

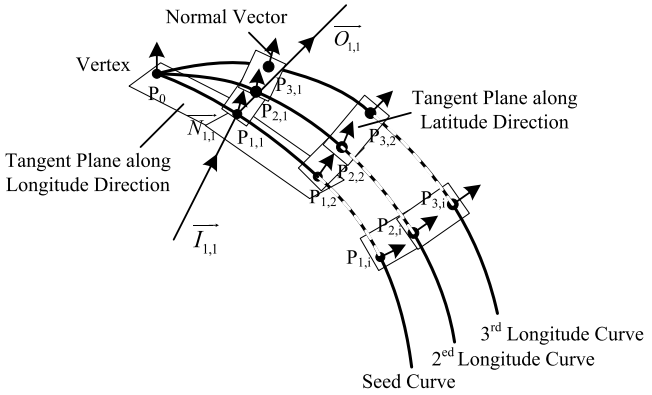

Figure 3. Schematic of point generation on the outside surface of the lens.

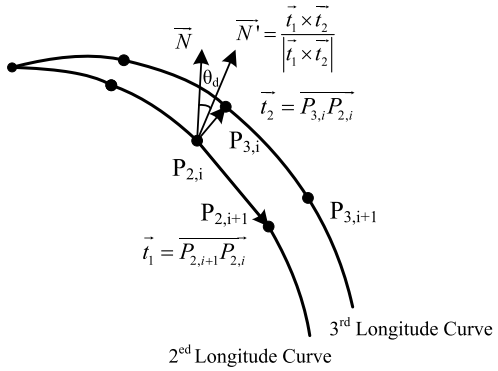

Figure 4. Deviation between the real unit normal vector ($\mathbf{N}'$) and the calculated unit normal vector ($\mathbf{N}$) of one point on the surface.

3.2. Construction of lens

In this section we will determine the lens which can realize the mapping between the light source and the target plane. There are four main steps to construct the outside surface of the freeform lens:

Step 1. Construction of the seed curve. The seed curve is the first curve to generate other lens curves and we will construct curves along the longitudinal direction. As shown in figure 3, we fix a point P_0 as the vertex of the seed curve. The first subscript of a point designates the sequence number $(1, 2, \ldots, M + 1)$ of the longitudinal curve and the second designates the sequence number $(1, 2, \ldots, N)$ of the point on a longitudinal curve except the vertex. The second point $P_{1,1}$ is calculated by the intersection of incident ray $\mathbf{I}_{1,1}$ and the tangent plane of the previous point. The direction of the refracted ray $\mathbf{O}_{1,1}$ can also be obtained as $\mathbf{Q}_1 - \mathbf{P}_{1,1}$, where Q_1 is the corresponding point of incident ray $\mathbf{I}_{1,1}$ on the target plane. Then we can obtain the normal vector $\mathbf{N}_{1,1}$ of the second point according to Snell's law expressed as follows:

$$[1 + n^2 - 2n(\mathbf{O} \cdot \mathbf{I})]^{1/2}\mathbf{N} = \mathbf{O} - n\mathbf{I} \tag{8}$$

where $\mathbf{I}$ and $\mathbf{O}$ are the unit vectors of incident and refracted rays, $\mathbf{N}$ is the unit normal vector on the refracted point and n is the refraction index of the lens. Based on this algorithm we can obtain all other points and their normal vectors on the seed curve. This method can guarantee that the tangent vectors of the seed curve are perpendicular to its calculated normal vectors.

Step 2. Generation of other longitudinal curves. Since the one-quarter light source is divided into M parts along the latitudinal direction, there are M corresponding longitudinal curves to be calculated except for the first seed curve. First of all we calculate the second curve whose vertex coincides with that of the seed curve. As shown in figure 3, different from the seed curve algorithm, point $P_{2,i}$ on the second longitudinal curve is calculated by the intersection of the incident ray and the tangent plane of point $P_{1,i}$ on the previous curve. Then the following longitudinal curves, such as the third curve, fourth curve, etc, are easy to obtain based on this algorithm.

Step 3. Error control. The unit normal vector ($\mathbf{N}$) of each point is calculated based on the corresponding incident ray and exit ray at that point. However, the surface construction algorithm of lofting between curves cannot guarantee the real unit normal vector ($\mathbf{N}'$) of the point of the lens surface is still the same as the calculated one ($\mathbf{N}$) [9]. Thus the direction of the exit ray will deviate from the expected one, which will result in poor illumination performance. As shown in figure 4, starting from the second longitudinal curve, every point (e.g. $P_{2,i}$) on the curve has only one adjacent point (e.g. $P_{3,i}$) on its tangent plane in the latitudinal direction. Therefore deviations between the real normal vectors and calculated ones are generated on these longitudinal curves. The deviation can be estimated by the deviation angle θ_d:

$$\theta_d = \cos^{-1}\left(\frac{\mathbf{N} \cdot \mathbf{N}'}{|\mathbf{N}||\mathbf{N}'|}\right). \tag{9}$$

Since θ_d becomes larger with the increase of the sequence of longitudinal curves, a threshold θ_{dth}, for example 6°, is needed to confine the deviation. If the maximum deviation of one longitudinal curve is larger than θ_{dth}, we go back to Step 1 and calculate another seed curve to replace this longitudinal curve.

Step 4. Construction of surface. The lofting method [14] is utilized to construct a smooth surface between these longitudinal curves. Since the newly generated seed curves are discontinuous with the longitudinal curves before them, the surface of the lens becomes discontinuous.

3.3. Validation of lens design

Since it is costly to manufacture a real discontinuous freeform lens, numerical simulation based on the Monte Carlo ray tracing method is an efficient way to validate the lens design. According to the simulation results, slight modification by trial and error is needed to make the illumination performance better. For instance, the construction of the transition surface between two sub-surfaces is not contained in this method, and the shape of the transition surface should be modified according to the simulation results and manufacturing process.

4. A design example

In this study, to meet the requirements of tunnel illumination, according to this design method, one discontinuous freeform

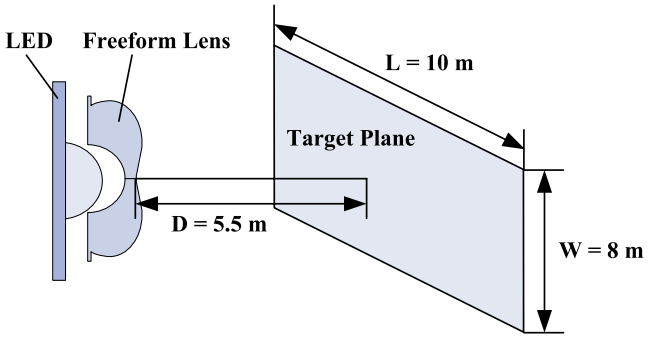

Figure 5. Schematic of the design target.

lens will be designed as an example for one LED to form a 10 m long and 8 m wide uniform rectangular illumination area at a height of 5.5 m (as shown in figure 5). The material of this lens is polymethyl methacrylate (PMMA) with a refractive index of 1.49. It is important to note that this method could also be used to design rectangular light patterns with different length–width ratios for other applications.

4.1. Optical modeling for an LED

In this study, as shown in figure 7, we used Cree® XLamp® XR-E LED as the light source due to it being one of the most popular LEDs in the market and its LIDC is special and more complicated than others, which makes it a good example to evaluate this algorithm. A point source optical model of Cree® XLamp® XR-E LED is to be established to evaluate this freeform lens design algorithm. However, illumination performance probably will deteriorate in practical applications since the size of the LED could not be ignored. Thus a practical optical model of Cree® XLamp® XR-E LED is also to be established to evaluate the actual illumination performance of the designed lens.

4.1.1. Optical modeling for a point light source. The LIDC of Cree® XLamp® XR-E LED is shown in figure 6 and it will be adopted as the light energy distribution of a point source during simulation. For designing an efficient freeform lens, the angular resolution of the LED LIDC measurement should be less than 1°.

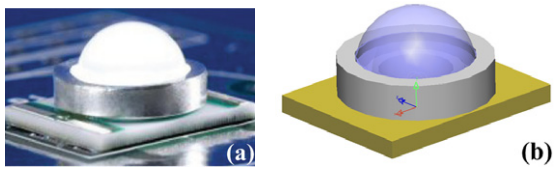

Figure 7. Cree® XLamp® XR-E LED: (a) material object and (b) practical optical model.

4.1.2. Optical modeling for a practical LED. First of all, we made some measurements to determine the geometrical parameters and established a practical structural model of the LED. We obtained the LIDC of this LED model by the widely used Monte Carlo ray tracing method and the LED was simulated by one million rays. Then, a precise LED optical model was established by comparing the similarity between the simulation LIDC and the experimental LIDC, which was quantified by the normalized cross-correlation (NCC) [15]. The NCC is written as in (10):

$$\mathrm{NCC} = \frac{\sum_x \sum_y (A_{xy} - \bar{A})(B_{xy} - \bar{B})}{\left[\sum_x \sum_y (A_{xy} - \bar{A})^2 \sum_x \sum_y (B_{xy} - \bar{B})^2\right]^{1/2}} \quad (10)$$

where A_{xy} and B_{xy} are the intensity or irradiance of the simulation value (A) and experimental value (B) and $\bar{A}$ ($\bar{B}$) is the mean value of A (B) across the x–y plane shown in figure 6. As for the modeling algorithm for an LED model mentioned in [16], we adjusted the scattering parameters and refraction indexes of some packaging materials used in LEDs, such as phosphor, polymer, silicone, etc, until the NCC reached as high as 97.6% (as shown in figure 8(a)). Thus, the precise optical modeling for the LED was finished.

4.2. Freeform lens design

One LED tunnel illumination freeform lens was designed according to this method. Firstly, we calculated a ten-order

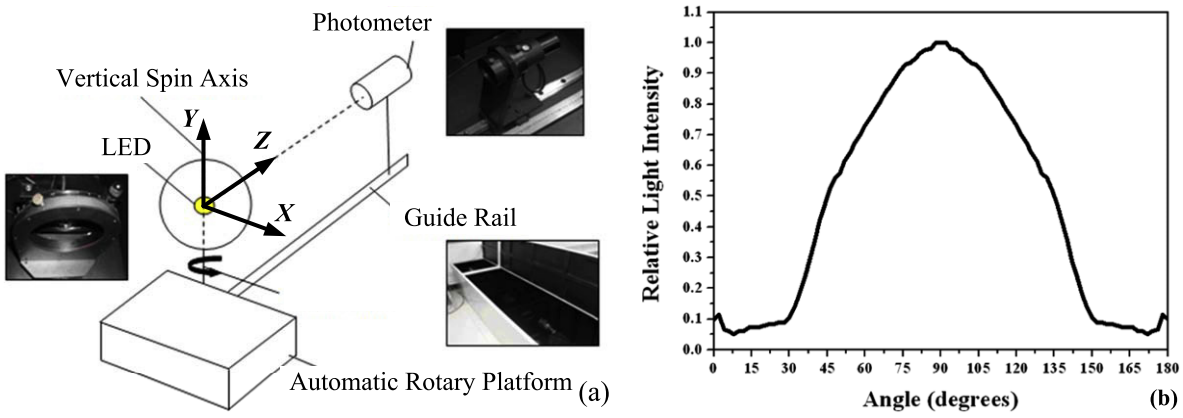

Figure 6. (a) Schematic of LIDC tester and (b) LIDC of Cree® XLamp® XR-E LED.

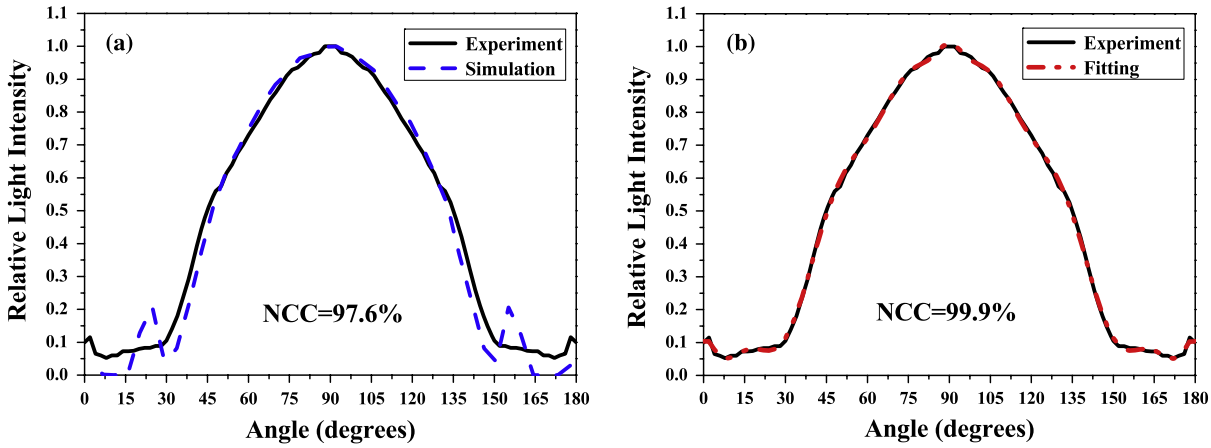

Figure 8. Experimental LIDC versus (a) simulation and (b) fitting for the Cree LED.

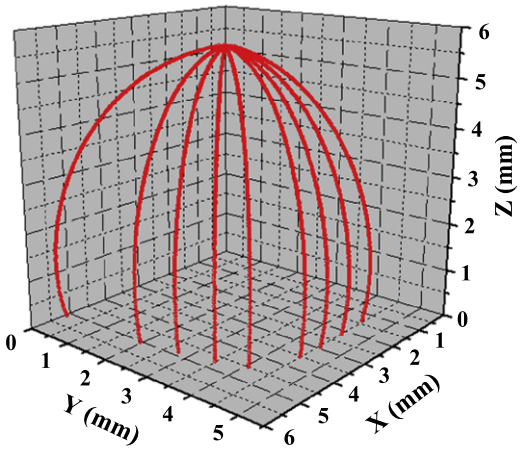

Figure 9. Seed curves of one-quarter discontinuous freeform lens.

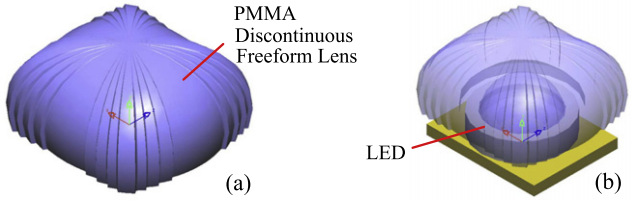

Figure 10. (a) PMMA discontinuous freeform tunnel lens and (b) a numerical model for Cree LED module with this lens.

polynomial to fit the tested LIDC according to the least-squares curve fitting method. Figure 8(b) depicts that the polynomial fits the test LIDC very well and the NCC reaches as high as 99.9%. Secondly, we divided the one-quarter light energy distribution of the light source and target plane both into 64 (M) $\times$ 500 (N) $=$ 32 000 grids with equal luminous flux and area, respectively, and established the light energy mapping relationship between these grids. Finally, we calculated the coordinates and normal vector of each point on the freeform surface and constructed the discontinuous freeform lens utilizing these points. We set the threshold θ_{dth} as 6° in our calculation and nine seed curves were constructed to reduce the deviation of exit rays. Figure 9 shows these seed curves and the sequence numbers of them are 1, 16, 22, 27, 31, 38, 42, 47 and 53, respectively[5]. As shown in figure 10(a), the whole discontinuous freeform lens was constructed by only 32 sub-surfaces, which makes it easier to manufacture and less manufacturing defects will be introduced compared with 450 sub-surfaces used in [10, 11]. The largest values of length, width and height of the lens are 10.6 mm, 9.7 mm and 5.1 mm, respectively.

[5] These seed curves can be supplied by contacting the authors.

4.3. Simulation illumination performance and tolerance analyses

The numerical illumination performance of the freeform lens using the point light source is shown in figure 11. This figure depicts simulation illuminance distributions on the test area with a size of 13 m long and 13 m wide that is 5.5 m away from the LED. From the simulation results, we can find that the lens forms a rectangular light pattern with a length of about 9.6 m and width of about 8.0 m, which is quite consistent with the design target. The LOE of the freeform lens is 97.4%. Fresnel loss is the main reason for light loss. The other light lost is mainly due to lens material absorption and total internal reflection (TIR) at the interface of lens and air. The uniformity, defined as $U = E_{\mathrm{min}}/E_{\mathrm{max}}$, across the center of the target plane along the X and Y axes are $U_X = 82.0\%$ and $U_Y = 81.3\%$, respectively. Since the shape of the light pattern will deteriorate sharply when there are some installation errors, we will calculate the uniformity within the area which is surrounded by sharp edges of the light pattern, for example, 9.6 m long and 8 m wide in figure 11.

The tolerance is an important issue for freeform lenses. In this study the tolerance analysis will be focused on increasing the size of the light source and installation errors, including migration and rotation of the lens.

The practical optical model for Cree® XLamp® XR-E LED with this freeform lens is shown in figure 10(b). The Cree EZ1000 LED chip is adopted in this LED module and its area is 0.98 mm $\times$ 0.98 mm. The phosphor is conformally coated on the chip with a thickness of about 50 μm. Considering the converted light, yellow light, irradiating from the phosphor

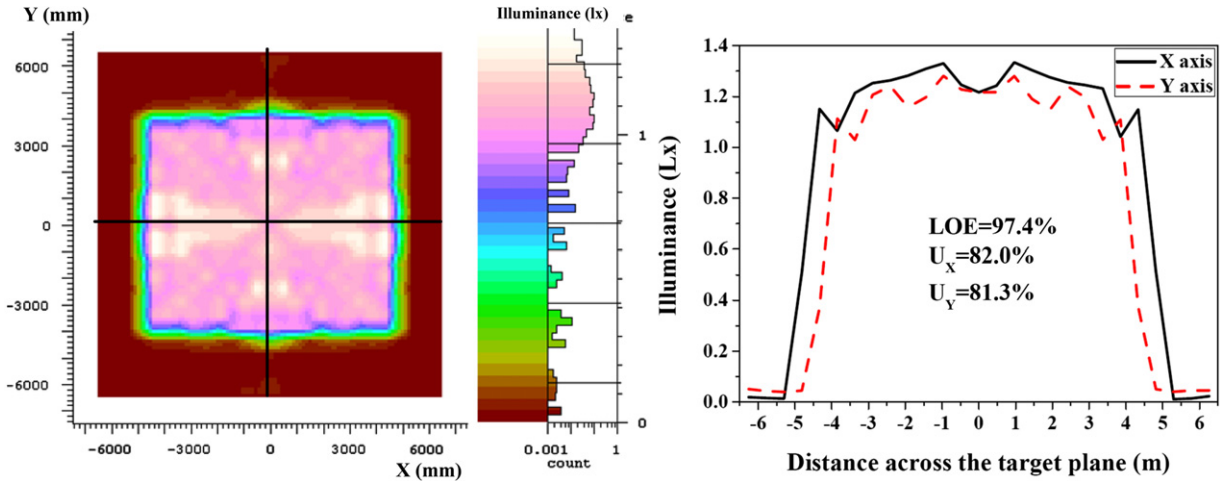

Figure 11. Numerical illumination performance of the freeform lens with a point light source.

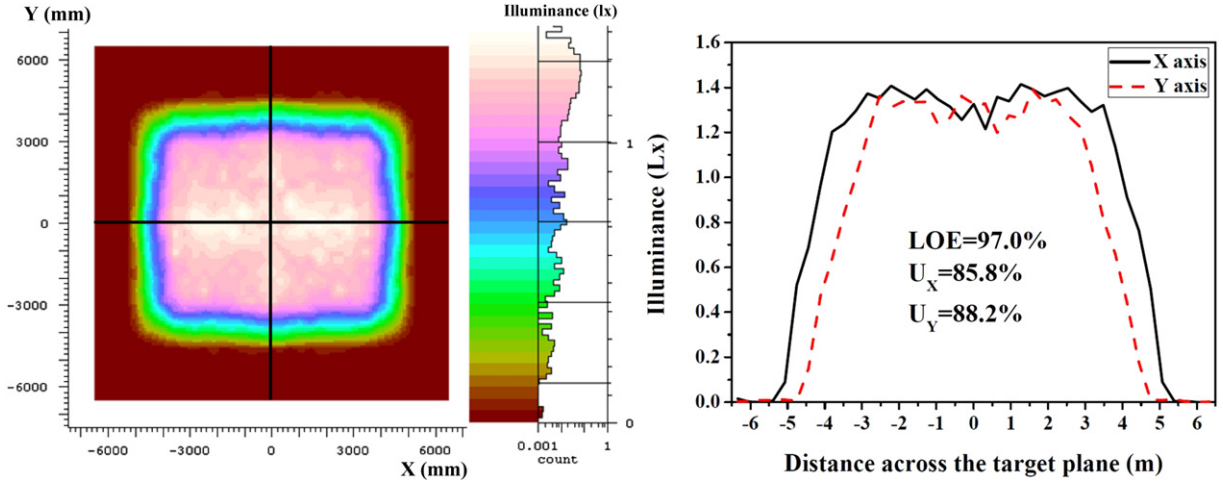

Figure 12. Numerical illumination performance of the freeform lens with practical Cree LED.

layer, the area of the light source in this Cree LED optical module is 1.08 mm × 1.08 mm. Since the distance from the chip to the outside surface of the lens is less than 5 times the chip size, this practical Cree LED could not be regarded as a point light source according to the far-field conditions of LEDs [17]. From simulation results shown in figure 12, we can find that, due to the increasing size of the light source, the edge of the light pattern becomes dim and the effective illumination area is decreased to 8.4 m long and 6.8 m wide, which is much smaller than that of the point light source condition. The LOE is still at a high level of 97.0% and U_X (U_Y) increases from 82.0% (81.3%) to 85.8% (88.2%). Therefore, increasing the size of the LED has little effect on the LOE of this discontinuous freeform lens, but significantly decreases the area of the light pattern. A large size LED chip is the development trend due to its high luminous flux of single LEDs. Thus, to limit the effect of the extended light source maximally, the size of the freeform lens should be enlarged correspondingly according to the far-field condition.

The effects of lens migration on the illumination performance are shown in figures 13 and 14. When the vertical deviation d_V of the lens increases from 0.2 to 0.6 mm, the LOE is still at a high level of more than 97.0%, but the light pattern becomes smaller and U_X (U_Y) declines from 85.8% (88.2%) to 61.7% (61.4%). Moreover, as shown in figure 14, the shape and uniformity of the light pattern both deteriorate sharply when the freeform lens deviates in the horizontal direction, except for LOE. Although the variation of U_Y is small, U_X declines from 85.8% to 60.2% as the horizontal deviation d_H increases up to 0.6 mm. Furthermore, the light pattern also becomes asymmetric and larger when d_H increases. Therefore, it seems that the illumination performance is more sensitive to installation errors in the horizontal direction.

The effects of lens rotation error were calculated as shown in figure 15. The illumination performance also deteriorates sharply when the rotation error of the freeform lens increases from 2° to 6°. The light pattern becomes larger and U_X declines from 85.8% to 53.7%, which is similar to the effects of installation errors in the horizontal direction.

The effects of installation errors on illumination performance are concluded in figure 16. Humans are distracted by an illuminance variation of about 33% across the target, thus the

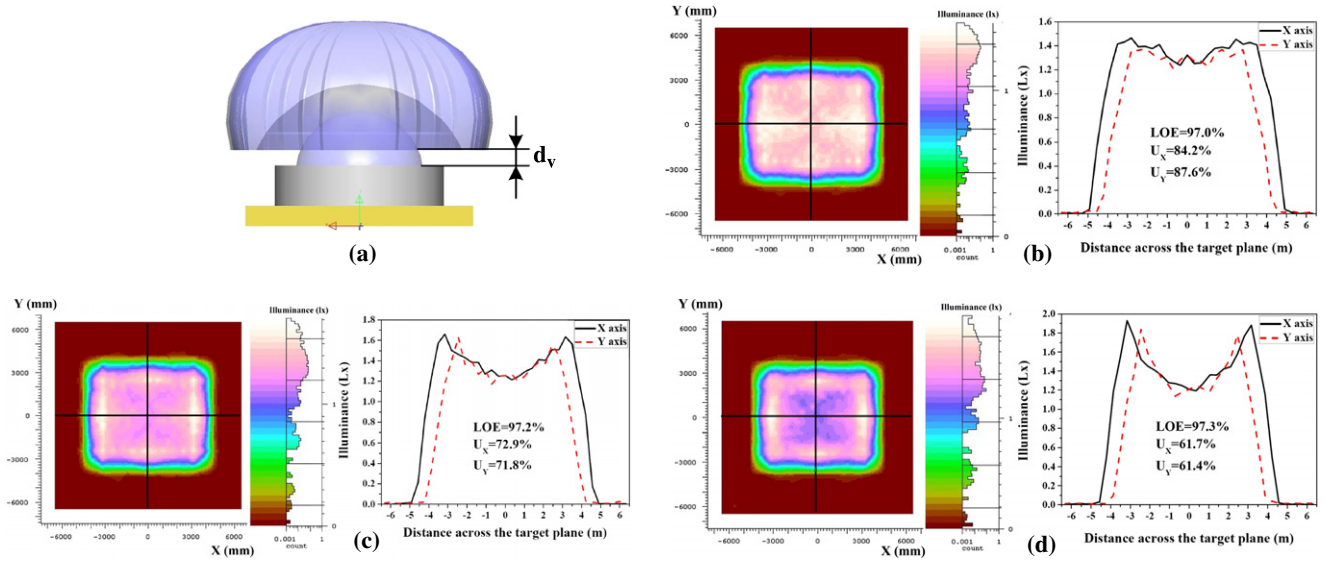

Figure 13. Effects of installation errors in the vertical direction: (a) schematic of vertical deviation d_V; (b) numerical illumination performance when $d_V = 0.2$ mm; (c) when $d_V = 0.4$ mm; and (d) when $d_V = 0.6$ mm.

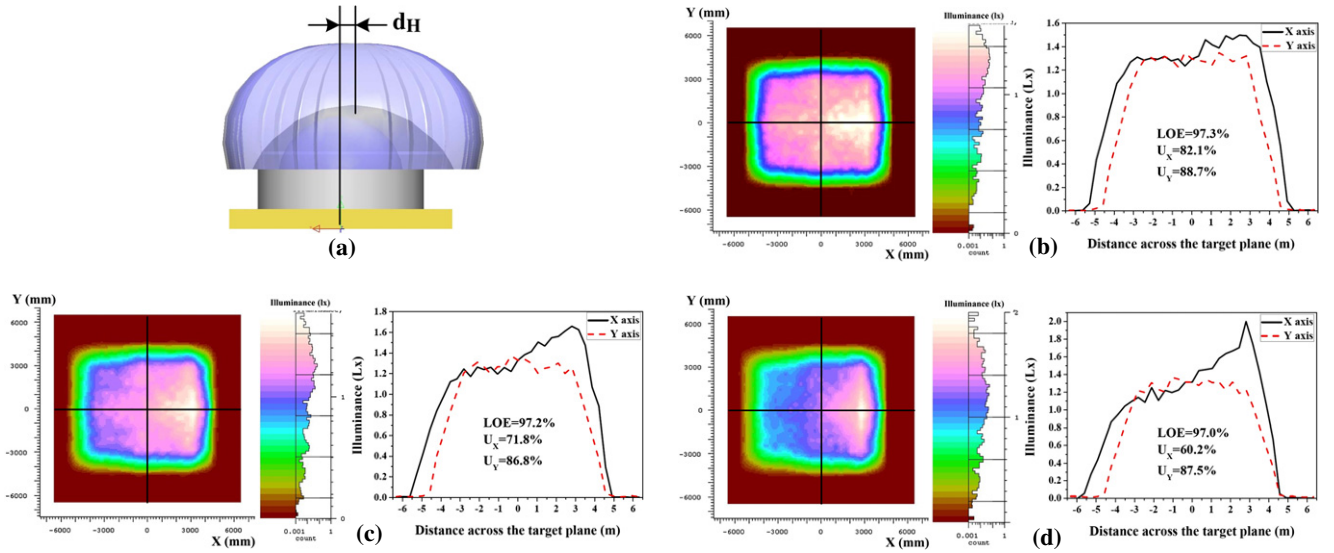

Figure 14. Effects of installation errors in the horizontal direction: (a) schematic of horizontal deviation d_H; (b) numerical illumination performance when $d_H = 0.2$ mm; (c) when $d_H = 0.4$ mm; and (d) when $d_H = 0.6$ mm.

illumination performance of a light pattern cannot be acceptable until the uniformity is larger than 67% either in the X or Y direction. From comparisons as shown in figure 16 we can find that the limits on the tolerance of vertical deviation, horizontal deviation and rotational error are 0.4 mm, 0.4 mm and 2°, respectively.

Variability of the LIDC caused by LED manufacturing defects is also an important issue to affect the illumination performance of the freeform lens. However, due to the limit of the polynomial fitting method, we cannot obtain variations of the LIDC profiles realistically and do not discuss the effects of variability of the LIDC on the illumination performance in this paper. Moreno *et al* [18] provided a better method to describe the LIDC of LEDs as the sum of a maximum of two or three Gaussian or cosine-power functions. By using this method, random variations of the LIDC profiles can be obtained realistically and tolerance analysis on the variability of the LIDC could be studied in future work.

5. Conclusions

In this study, a modified discontinuous freeform lens design method was presented for rectangularly prescribed illumination, with the advantages of a flexible energy mapping relationship, accurate light irradiation control and easier to manufacture. A PMMA discontinuous freeform lens, constructed by only 32 sub-surfaces, was designed as an example for high quality LED tunnel illumination according to this method. The numerical simulation results demonstrated

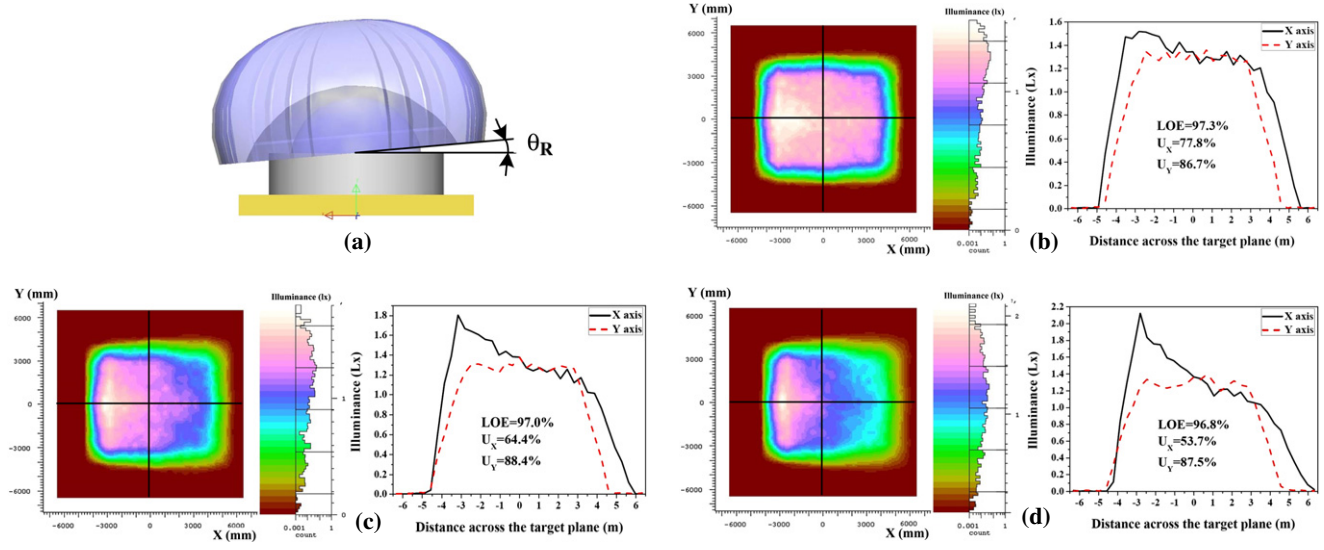

Figure 15. Effects of installation errors of rotation: (a) schematic of rotation angle θ_R; (b) numerical illumination performance when $\theta_R = 2°$; (c) when $\theta_R = 4°$; and (d) when $\theta_R = 6°$.

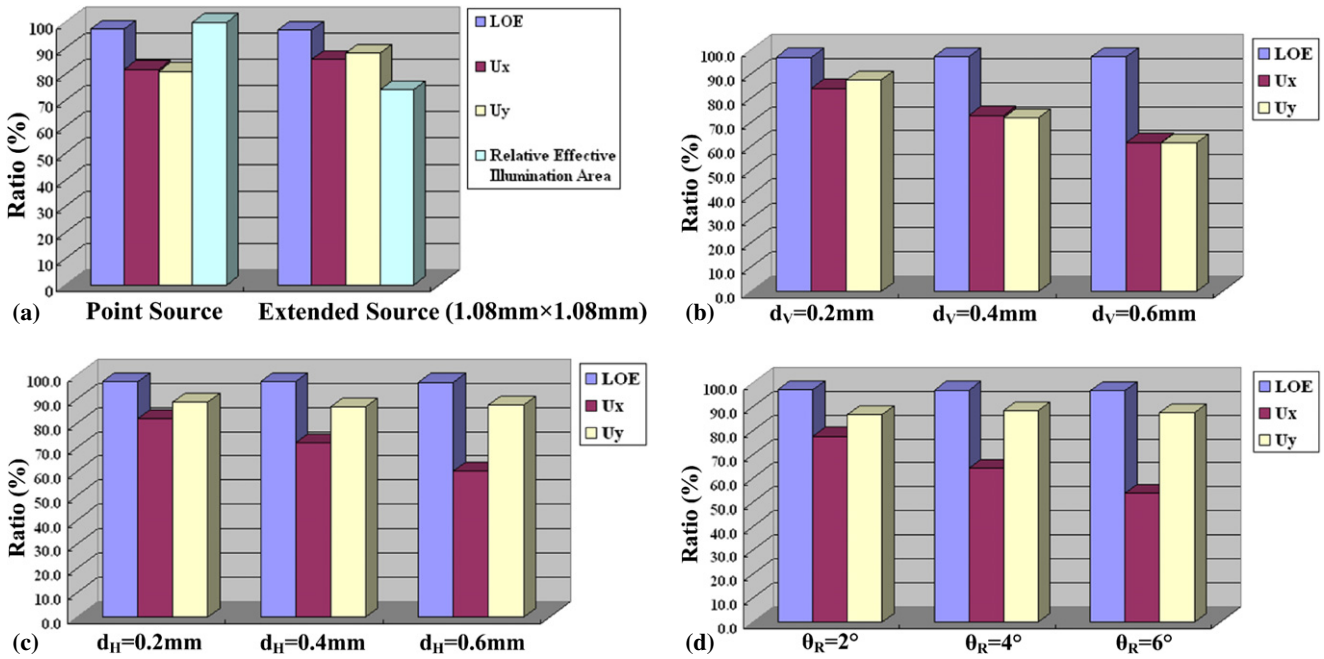

Figure 16. Comparisons of effects of increasing size of light source and installation errors on illumination performance.

that the light pattern of the lens was in very good agreement with the expected illumination performance when using a point source. Tolerance analyses were also conducted. The extended light source had little effect on the LOE of the lens but significantly decreased the effective illumination area. Installation errors had much more effect on the uniformity and shape of the light pattern than the light output efficiency of the lens. The tolerances of vertical deviation, horizontal deviation and rotational error of the lens were 0.4 mm, 0.4 mm and 2°, respectively. This modified method has a potential to be widely used in other applications, such as LED backlighting, streetlighting, etc. However, the Fresnel loss and TIR loss should be included in the design method in future to enhance the LOE of the lens further. Moreover, effects of the variability of the LEDs' LIDC and manufacturing defects on the illumination performance should also be considered in future work.

Acknowledgments

This work was supported by the Nature Science Foundation of China (NSFC) Key Project under grant no. 50835005, the NSFC Project under grant no. 50876038, the High Tech Project of the Ministry of Science and Technology under grant no. 2008AA03A184 and GuangDong Real Faith Optoelectronics Inc.

References

[1] Schubert E F 2006 *Light-Emitting Diodes* (Cambridge: Cambridge University Press)

[2] Evans D L 1997 High-luminance LEDs replace incandescent lamps in new applications *Proc. SPIE* **3002** 142–53

[3] Chen G, Craven M, Kim A, Munkholm A, Watanabe S, Camras M, Götz W and Steranka F 2008 Performance of high-power III-nitride light emitting diodes *Phys. Status Solidi* a **205** 1086–92

[4] Winston R, Miñano J C and Benítez P 2005 *Nonimaging Optics* (San Diego: Elsevier Academic) pp 181–218

[5] Benítez P, Miñano J C, Blen J, Mohedano R, Chaves J, Dross O, Hernández M and Falicoff W 2004 Simultaneous multiple surface optical design method in three dimensions *Opt. Eng.* **43** 1489–502

[6] Ries H and Muschaweck J 2002 Tailored freeform optical surfaces *J. Opt. Soc. Am.* A **19** 590–5

[7] Parkyn W A 1998 The design of illumination lenses via extrinsic differential geometry *Proc. SPIE* **3428** 154–62

[8] Parkyn W A 1999 Segmented illumination lenses for step lighting and wall-washing *Proc. SPIE* **3779** 363–70

[9] Wang L, Qian K Y and Luo Y 2007 Discontinuous free-form lens design for prescribed irradiance *Appl. Opt.* **46** 3716–23

[10] Ding Y, Liu X, Zheng Z R and Gu P F 2008 Freeform LED lens for uniform illumination *Opt. Express* **16** 12958–66

[11] Ding Y, Liu X, Zheng Z R and Gu P F 2008 Secondary optical design for LED illumination using freeform lens *Proc. SPIE* **7103** 71030K

[12] Hao X, Zheng Z R, Liu X and Gu P F 2008 Freeform surface lens design for uniform illumination *J. Opt. A: Pure Appl. Opt.* **10** 075005

[13] Ries H and Rabl A 1994 Edge-ray principle of nonimaging optics *J. Opt. Soc. Am.* A **11** 2627–32

[14] Piegl L and Tiller W 1997 *The NURBS Book* 2nd edn (Berlin: Springer)

[15] Sun C C, Lee T X, Ma S H, Lee Y L and Huand S M 2006 Precise optical modeling for LED lighting verified by cross correlation in the midfield region *Opt. Lett.* **31** 2193–5

[16] Wang K, Luo X B, Liu Z Y, Zhou B, Gan Z Y and Liu S 2008 Optical analysis of an 80 W light-emitting-diode street lamp *Opt. Eng.* **47** 013002

[17] Moreno I and Sun C C 2008 LED array: where does far-field begin? *Proc. SPIE* **7058** 70580R

[18] Moreno I and Sun C C 2008 Modeling the radiation pattern of LEDs *Opt. Express* **16** 1808–19